CDK9 Inhibition Induces a Metabolic Switch that Renders Prostate Cancer Cells Dependent on Fatty Acid Oxidation

Harri M. Itkonen[*,†], Ninu Poulose[§], Suzanne Walker[†] and Ian G. Mills[*,§,¶]

[*]Centre for Molecular Medicine Norway, Nordic European Molecular Biology Laboratory Partnership, Forskningsparken, University of Oslo, Oslo, 0349, Norway; [†]Department of Microbiology, Blavatnik Institute, Harvard Medical School, Boston, MA, 02115, USA; [‡]PCUK/ Movember Centre of Excellence for Prostate Cancer Research, Centre for Cancer Research and Cell Biology (CCRCB), Queen's University Belfast, BT7 1NN, UK; [§]Nuffield Department of Surgical Sciences, University of Oxford, John Radcliffe Hospital, Oxford, OX3 9DU, UK

Abstract

Cyclin-dependent kinase 9 (CDK9), a key regulator of RNA-polymerase II, is a candidate drug target for cancers driven by transcriptional deregulation. Here we report a multi-omics-profiling of prostate cancer cell responses to CDK9 inhibition to identify synthetic lethal interactions. These interactions were validated using live-cell imaging, mitochondrial flux-, viability- and cell death activation assays. We show that CDK9 inhibition induces acute metabolic stress in prostate cancer cells. This is manifested by a drastic down-regulation of mitochondrial oxidative phosphorylation, ATP depletion and induction of a rapid and sustained phosphorylation of AMP-activated protein kinase (AMPK), the key sensor of cellular energy homeostasis. We used metabolomics to demonstrate that inhibition of CDK9 leads to accumulation of acyl-carnitines, metabolic intermediates in fatty acid oxidation (FAO). Acyl-carnitines are produced by carnitine palmitoyltransferase enzymes 1 and 2 (CPT), and we used both genetic and pharmacological tools to show that inhibition of CPT-activity is synthetically lethal with CDK9 inhibition. To our knowledge this is the first report to show that CDK9 inhibition dramatically alters cancer cell metabolism.

Neoplasia (2019) 21, 713–720

Introduction

Uncontrolled growth of cancer cells requires significant metabolic reprogramming to satisfy the requirements of rapidly dividing cells. Most cancers have increased appetite for glucose, which allows evaluation of the tumor-burden using glucose-positron emission tomography (PET) [1]. Prostate cancer, the most common cancer in males in the USA [2], is not always readily detectable using PET-imaging, but can instead be visualized using ^{11}C-acetate due to higher dependency of prostate cancer cells on lipids for energy production [3,4].

Normal prostate tissue and prostate cancer have specific metabolic features that are distinct from the rest of the body. In the untransformed state, cells of the prostate gland accumulate high levels of citrate due to prostate-specific accumulation of zinc [5,6]. High zinc concentration inhibits m-aconitase activity and citrate oxidation, truncating the TCA cycle and reducing ATP production [7]. Some of the prostate-specific metabolic features may be utilized to sensitize prostate cancer cells to other treatments.

Cell division requires a substantial amount of ATP and continuous synthesis of macromolecules, especially nucleic acids and lipids. Direct crosstalk between metabolism and the cell-cycle regulators, cyclin-dependent kinases (CDKs), could integrate nutrient

availability with cell proliferation. There is clear evidence of such crosstalk in the literature. For example, increased glucose uptake can activate oncogenic signaling in nonmalignant cells [8]. Conversely, CDK1, the major regulator of the G2/M cell cycle transition is also targeted to mitochondria, where it phosphorylates proteins of the complex 1 electron-transport machinery to promote ATP production [9]. In addition, CDK4 and CDK6, regulators of the G1-S transition, can also directly regulate glucose metabolism [10,11]. Increased activity of CDKs is observed in most cancers, which has fostered development of CDK inhibitors for cancer therapy.

Regulation of cell cycle initiation and progression is ultimately dictated through transcriptional regulation. A specific class of CDKs phosphorylate the RNA-polymerase II (RNA-Pol II) carboxy-terminal domain (CTD) to regulate its activity [12,13]. CDK7 and CDK9 are the major RNA-Pol II CDKs. CDK7 promotes transcription initiation, while the switch to productive elongation is dependent on CDK9. CDK7 additionally functions as a CDK-activating kinase and inhibition of its activity will directly affect both cell cycle CDKs and RNA-Pol II [14]. On the other hand, CDK9 has a well-defined primary function, and several reports suggest that this enzyme could be an attractive target for prostate cancer therapy. First, CDK9-mediated phosphorylation regulates the activity of the androgen receptor, the major drug-target in prostate cancer [15]. Second, CDK9 is required for RNA-Pol II pause-release, a process that is frequently deregulated in cancer cells [16,17]. Third, compounds targeting CDK9 induce apoptosis in cancer cells, in part through decreased expression of the anti-apoptotic proteins [18]. These data position CDK9 as an attractive target for cancer therapy.

In this study, we show that the pan-CDK inhibitor AT7519 induces acute metabolic stress in prostate cancer cells. Metabolite profiling showed that AT7519 treatment led to accumulation of acyl-carnitines. We identify CDK9 as the key mediator of the observed metabolic effects in prostate cancer cells and show that simultaneous inhibition of CDK9 and enzymes required for acyl-carnitine production (CPT1 and CPT2) is lethal to prostate cancer cells. In brief, our study reports a CDK9 inhibition-in-duced adaptive metabolic response in prostate cancer cells, and thereby identifies a candidate compound combination for prostate cancer therapy.

Materials and Methods

Cell Culture and Manipulations

LNCaP and PC3 cells were obtained from ATCC and maintained as recommended by the provider. AT7519 (used in a dose of 0.5 μM unless otherwise indicated) and Etomoxir were purchased from Selleckchem. Perhexiline (used in a dose of 10 μM unless otherwise indicated) was purchased from Sigma. NVP2 was from MedChem Express. Viability assays were performed using the CellTiter-Glo Luminescent Cell Viability Assay (Promega). Growth rate and cell death activation were evaluated using the Incucyte instrument according to manufacturer's instructions. For detection of cell death activation, we used IncuCyte Caspase-3/7 Green Reagent for Apoptosis (Essen Biosciences). Cell cycle analysis was performed using the Propidium Iodide Flow Cytometry Kit (Abcam, ab139418) and the BD FACSCanto instrument (BD Biosciences). Knockdown experiments were performed using RNAiMax reagent (Sigma). CPT1

targeting siRNAs were from ThermoFisher Scientific (siCPT1a s3467 and siCPT2 s3468).

Seahorse Metabolic Flux Analysis

Metabolic flux analysis was performed using a Seahorse XFe 96 instrument. An equal number of LNCaP cells were plated and allowed to attach for 1 day. Cells were treated with inhibitors for 24 hours and subjected to flux analysis. In brief, cells were changed to base media containing 1 mM pyruvate, 2 mM glutamine and 10 mM glucose 45 minutes before the assay. Cartridge was equilibrated overnight and loaded with Oligomycin 2 μM, FCCP 1 μM and rotenone/antimycin A 0.5 μM prior to the assay. Results were analyzed using Seahorse Wave software.

Protein Profiling

Samples for western blotting were prepared as previously described [19]. Samples for the reverse-phase protein array profiling were prepared using the same protocol. Antibodies used are as follows: from Cell Signaling Technology, Cl-PARP (9541), p-H2AX (9718), p-h3ser10 (9701), CPT1A (12252), h3 (9715), HES1 (11988), CDK1 (9116), p-RNA Pol II-Ser 2 (13499), MCL1 (5453 T) and MYC (5605S). Actin (ab49900), CPT2 (ab181114) and GAPDH (9485) antibodies were from Abcam.

mRNA Profiling

RNA isolation was performed using the illustraMiniSpin-kit (GE Healthcare) according to manufacturer's instructions, except luciferase RNA (Promega, cat # L4561) was added into cell lysis buffer. cDNA was synthesized using the qScript cDNA Synthesis Kit (Quantabio). Primers used are as follows: MYC F- TACCC TCTCAACGACAGCAG, R- TCTTGACATTCTCCTCGGTG; MCL1 F- TGCTTCGGAAACTGGACATCA, R-TAGCCACA AAGGCACCAAAAG and Luciferase F-TACAACACCCC AACATCTTCGA, R- GGAAGTTCACCGGCGTCAT.

Metabolomic Profiling

LNCaP cells were allowed to attach for 1 day and treated for 1 day. For harvesting, cells were washed with PBS, trypsinized, counted and centrifuged 4000 rpm for 5 minutes at 4 °C, washed with PBS, centrifuged again, pellet was washed with water (cells not solubilized), cells were frozen using liquid nitrogen and stored at –80 °C until analysis. Targeted metabolomics was purchased as a service from FIMM Metabolomics/Lipidomics/Fluxomics Unit (Helsinki Finland).

Results

CDK Inhibitor AT7519 Induces Acute Metabolic Stress in Prostate Cancer Cells

Cyclin-dependent kinase (CDK) inhibitors suppress cell cycle progression, but there has been no study on how the prostate cancer cell proteome is altered in response to CDK inhibition. In order to characterize these changes, we used AT7519, a pan-CDK-inhibitor that most potently targets CDK9 [20].

We wanted to identify both immediate and sustained changes in the proteome using reverse-phase protein arrays (RPPA), and therefore analyzed two time-points, 4 and 24 hours after treatment with AT7519. In order to identify adaptive changes that enable cell survival, we selected a dose (500 nM) that decreased the proliferation rate of cells but did not induce substantial cell death as measured by

live-cell imaging and PARP cleavage, respectively (Supplementary Figure 1, *A* and *B*). We hypothesized that proteins whose expression changes rapidly and in a sustained manner report on the most essential adaptations for cancer cell survival. We identified two targets whose levels were significantly increased at both time points, the phosphorylated form of AMP-activated protein kinase (AMPK) and the serine/threonine-protein kinase A-Raf (Figure 1*A* and Suppl. Table 1). Lopez-Mejia et al. (2017) have reported that CDK4-mediated phosphorylation of AMPK increases glycolysis and decreases fatty acid oxidation in mouse embryonic fibroblasts [21]. However, the RPPA-data showed that inhibition of CDK-activity using AT7519 induced phosphorylation of AMPK in prostate cancer cells. AMPK is one of the key regulators of cellular energy homeostasis and is canonically activated in response to an increased AMP/ATP ratio [22]. As detailed in the introduction, prostate cancer cells have unique metabolic features, and we speculated that phosphorylation of AMPK in response to AT7519 might represent a prostate cancer-specific metabolic response. We therefore focused on AMPK, and first confirmed by western blotting that AMPK phosphorylation is indeed induced in a dose-dependent manner in response to AT7519 treatment (Figure 1*B*). Activation of AMPK in response to AT7519 suggested that the treatment might decrease cells' ability to produce ATP.

We directly measured the cellular oxygen-consumption rate (OCR) to assess if AT7519 affects the rate of ATP production. AT7519

dose-dependently inhibited mitochondrial oxygen consumption and ATP production (Figure 1, *C* and *D*). Basal respiration-, maximal respiration- and proton leak-dependent OCR were also decreased, but coupling efficiency was maintained. These data indicate that the activity of the mitochondria decreases in response to AT7519 treatment, but the mitochondria remain functional.

We have so far shown that a low dose of AT7519 induces acute metabolic stress in prostate cancer cells. The dose selected led to a strong decrease in cells' ability to produce ATP but did not induce apparent cell death. We therefore hypothesized that cells activate alternative metabolic strategies to enable survival in the presence of AT7519.

AT7519 Induces Accumulation of Acyl-Carnitines

We performed metabolite profiling to probe the possibility that AT7519 affects metabolites involved in ATP generation. Targeted mass spectrometry was used to quantify ~100 different metabolites, including amino acids, nucleotides, neurotransmitter intermediates, choline metabolites and enzyme cofactors (Figure 2*A*). We noted a prominent decrease in nucleotide metabolites, including uracil (–51%), hypoxanthine (–40%), inosine (–29%) and guanosine (–20%). In addition, AT7519 induced a striking increase in the abundance of the nine different acyl-carnitines measured (Figure 2, *A* and *B*). Carnitine serves as an acyl-group carrier across the mitochondrial membrane in a process that delivers lipids to mitochondria for fatty acid oxidation [23]. The metabolite profiling
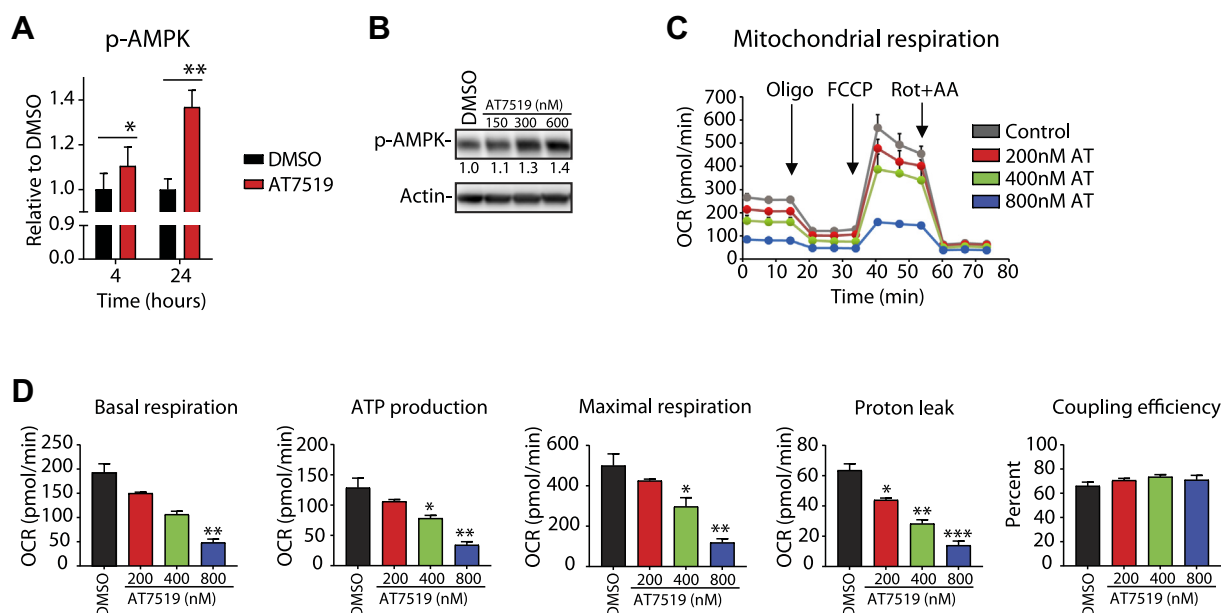
Figure 1. AT7519 treatment induces acute metabolic stress. **A)** AMPK phosphorylation in response to AT7519 in LNCaP cells. Data was recorded using the reverse-phase protein array (RPPA)-approach (all the data is provided in Suppl. Table 1). LNCaP cells were treated with 0.5 µM AT7519 for 4 and 24 hours and cell lysates were analyzed using RPPA profiling. Data shown is an average of four biological replicates with SEM and Student's *t*-test was used to evaluate statistical significance (*<.05, **<.01). **B)** LNCaP cells were treated with DMSO or increasing dose of AT7519 for 24 hours and samples were analyzed using western blotting. Densitometry was used to evaluate the abundance of each protein. This is a representative western blot of two replicates. **C, D)** AT7519 treatment decreases mitochondrial oxygen-consumption rate (OCR) in LNCaP cells. Cells were treated with either DMSO or AT7519 for 24 hours prior to start of the Seahorse XFe 96 analyzer OCR-measurements. Serial injections of oligomycin (Olig), Carbonyl cyanide-p-trifluoromethoxyphenylhydrazone (FCCP), and a mix of rotenone and antimycin (Rot+AA) enabled measurements of ATP production, maximal respiration, and non-mitochondrial respiration, respectively. Proton leak and spare respiratory capacity were calculated using these parameters and basal respiration. Data shown is an average of 3–4 biological replicates with SEM and Student's *t*-test was used to assess the statistical significance (*<.05, **<.01, ***<.001).
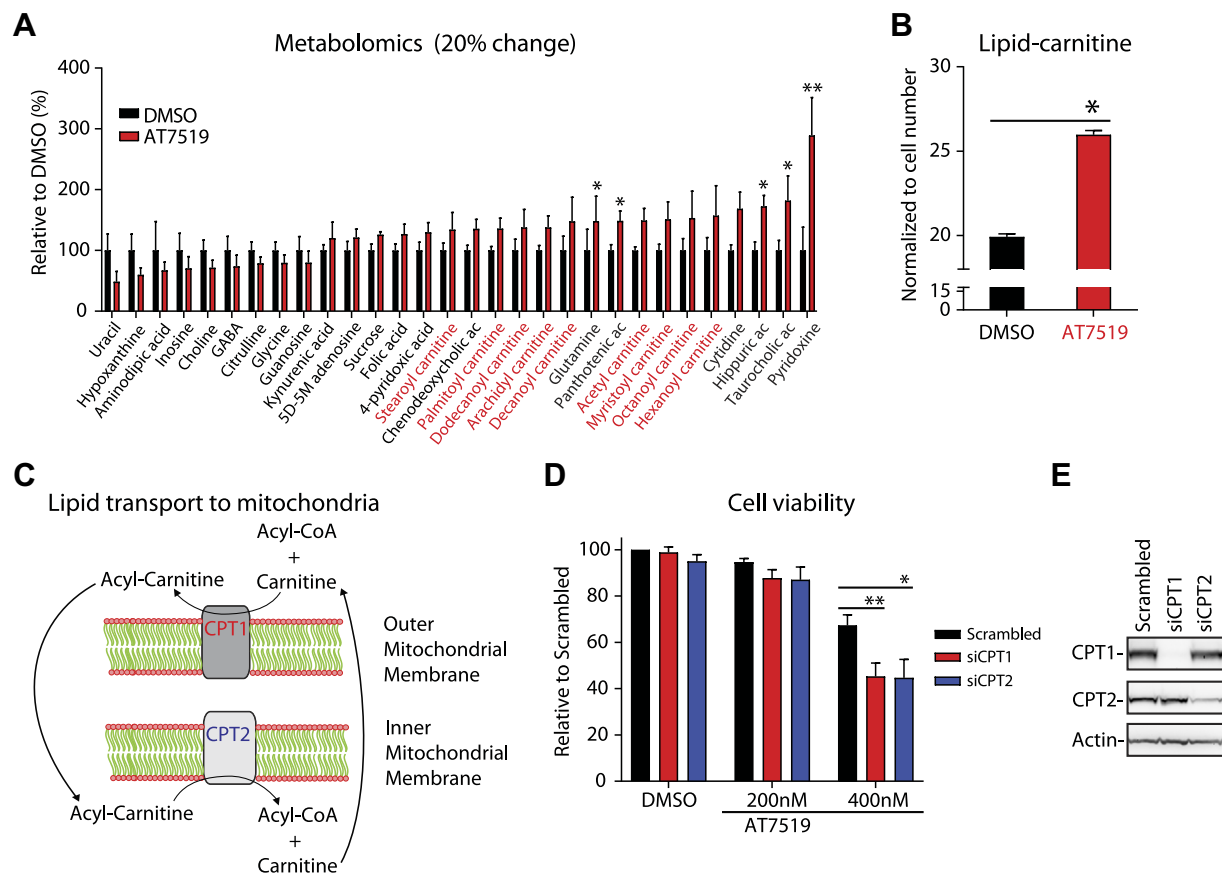
Figure 2. AT7519 induced accumulation of acyl-carnitines promotes prostate cancer cell survival. **A)** Targeted metabolite profiling of LNCaP cells treated as indicated for 24 hours. Data shown is an average of four biological replicates with SEM. Only metabolites whose abundance changed at least 20% in comparison to DMSO are shown. Metabolite levels were quantitatively measured using mass spectrometry and normalized to cell count. Control sample was set to 100% and treatments were also normalized to this. Student's t-test was used to assess the statistical significance (*<.05, **<.01). **B)** Measurement of the absolute amount of carnitines. Data shown is an average of 4 biological replicates with SEM and t-test was used to evaluate the statistical significance (*<.05). **C)** Schematic presentation of acyl-carnitine transport across the mitochondrial membrane. **D)** Knockdown (KD) of CPT1 and CPT2 sensitizes cells to AT7519 treatment. KD was performed for 4 days as indicated, after which cells were treated with AT7519 for 3 days and viability was assessed using the CellTiter-Glo assay. Data shown is an average of at least 3 biological replicates with SEM and t-test was used to evaluate the statistical significance (*<.05, **<.01). **E)** The efficacy of CPT1 and CPT2 KD was evaluated using western blotting.

data suggest that AT7519 reprograms cells to rely more on fatty acid oxidation.

We tested if the accumulation of acyl-carnitines in response to AT7519-treatment is important for cancer cell survival. Addition and removal of the lipid chain to and from carnitine is catalyzed by carnitine palmitoyltransferases (CPT) 1 and 2, which are localized in the outer and inner mitochondrial membranes, respectively [23] (Figure 2C). These enzymes are required for acyl-carnitine production and fatty acid oxidation, and we tested if they are part of the adaptive response to AT7519. Knockdown of either CPT1 or CPT2 sensitized cells to AT7519 (Figure 2, D and E).

In summary, AT7519-treatment leads to depletion of nucleotide intermediates and accumulation of acyl-carnitines, and knockdown of the CPT enzymes sensitizes cells to AT7519. Therefore, acyl-carnitine accumulation appears to be an adaptive response to AT7519 treatment that promotes survival of cancer cells and represents a metabolic switch that can be targeted. We next set out to test if synthetic lethality between CDK inhibition and CPT inhibition could be achieved through pharmacological approaches, which would be applicable in a clinical setting.

AT7519 and Inhibitors of Fatty Acid Oxidation are Synthetically Lethal to Prostate Cancer Cells

In order to probe if AT7519 renders prostate cancer cells dependent on lipids for ATP synthesis, we pre-treated cells with AT7519 and measured mitochondrial oxygen consumption in response to acute treatment with Perhexiline, a clinically approved CPT inhibitor [24]. Indeed, acute treatment with Perhexiline decreased the mitochondrial oxygen consumption of cells pretreated with AT7519 (Figure 3A). This result is consistent with our model that AT7519 renders prostate cancer cells more dependent on lipids for ATP synthesis and this dependency can be targeted using Perhexiline.

We next assessed the effects of combination treatment with AT7519 and CPT inhibitors on viability of prostate cancer cells. Perhexiline and Etomoxir, another FAO-inhibitor [25], dose-dependently decreased prostate cancer cell viability as assessed by ATP generation, and co-treatment with AT7519 additively enhanced their effects (Supplementary Figure 2, A and B). Etomoxir is an irreversible inhibitor of CPT1 and the compound has been used to inhibit fatty acid oxidation in both normal and cancer cells,

however, its specificity in higher doses has been questioned [26–30]. In this context, it is important to keep in mind that we have demonstrated the anti-proliferative effect of combining AT7519 and fatty acid oxidation inhibition not only by using Etomoxir, but also by using Perhexiline (Supplementary Figure 2, *A* and *B*) and by knocking down CPT1 and CPT2 (Figure 2*D*). Combining Perhexiline with AT7519 led to a complete loss of cell viability in LNCaP and PC3 cells (Supplementary Figure 2*B*), and this compound was selected for the future experiments.

We have shown that the metabolic adaptations induced by AT7519 and Perhexiline converge to decrease cell viability and searched the literature for clues to other mechanisms of decreased cell survival besides ATP depletion, which is clearly a factor. Inhibition of fatty acid oxidation has been shown to increase the levels of reactive oxygen species (ROS) [31], and earlier we noted that AT7519-treatment causes depletion of nucleotide precursors (Figure 2*A*). ROS accumulation and unbalanced nucleotide levels are known to cause DNA damage [32]. We therefore evaluated if the AT7519-Perhexiline combination induces DNA damage using western blot. Combining AT7519 with Perhexiline caused a greater than 9-fold enhanced induction of the canonical DNA-damage marker p-H2AX (Figure 3*B*). To further probe the mechanistic basis of the AT7519-Perhexiline combination on viability, we evaluated cell cycle distribution using propidium iodide-staining and flow cytometry. Treatment with the compound combination led to a greater than 5-fold increase in the sub-G1 population of cells (Figure 3*C*). A similar effect on the cell cycle was observed in PC3 cells, another prostate cancer cell line (Supplementary Figure 2*C*). Therefore, the perhexiline-AT7519 combination induced decrease in cell viability is explained by depletion of ATP, excessive DNA damage and possibly by the activation the cell death response.

We assessed if the AT5719-Perhexiline combination induces apoptosis by several assays. First, we performed western blotting and observed a greater than 5-fold increase in PARP cleavage with a concomitant decrease in the marker of mitotic cells, phosphorylated h3-ser10 (Figure 3*B*). Second, we used live-cell imaging to measure activation of caspases 3 and 7, the prototypical markers of apoptosis. Combination treatment led to a 6-times higher activation of caspases in LNCaP cells (Figure 3*D*). Third, we evaluated the proliferation rate of cells treated with AT7519, Perhexiline and the combination. In agreement with the prominent cell death activation, the combination treatment additively decreased proliferation of LNCaP cells (Figure 3*E*). In addition, the AT7519-Perhexiline combination induced cell death and resulted in growth arrest also in PC3 cells (Supplementary Figure 3, *A* and *B*). These data establish AT7519 and Perhexiline as a synthetically lethal compound combination to prostate cancer cells.

Simultaneous Targeting of CDK9 and Fatty Acid Oxidation is Synthetically Lethal to Prostate Cancer Cells

As with any studies involving chemical probes, it is important to test additional compounds that inhibit the same proposed targets, if possible. We found that Perhexiline and Etomoxir, as well as CPT knockdown, had similar effects on cells when combined with AT7519 (Figure 2*D* **and** Supplementary Figure 2, *A* and *B*). AT7519 is a pan-CDK inhibitor that most potently targets CDK9 [20], and we therefore hypothesized that CDK9 is the primary target for the combinatorial lethality between AT7519 and Perhexiline. In 2018, a novel CDK9 inhibitor, NVP2, was identified and reported to have 700-fold selectivity over other kinases [33]. We found that

treatment with NVP-2 led to a rapid (24 hours treatment), dose-dependent depletion of the cellular ATP-levels at low nanomolar concentrations (Figure 3*F*). In addition, and similar to AT7519, NVP2-treatment caused activation of AMPK and resulted in down-regulation of CDK1 and up-regulation of HES1 (Figure 3*G*). We noted that 10 nM NVP2 had only a modest effect on the phosphorylation of serine-2 of RNA Pol II CTD with clear effect on the ATP levels (Figure 3, *F* and *G*). It is possible that the ATP generation is very sensitive to CDK9 inhibition and in order to further probe if NVP2 decreases transcription also in low doses, we treated cells with NVP2 for 4 hours, isolated total RNA using cell lysis buffer that contains spike-in luciferase RNA for normalization and evaluated the transcript levels of MYC and MCL1, both of which have been reported to be affected by CDK9 inhibition [33,34]. Importantly, NVP2 decreased MYC and MCL1 mRNA levels by over 50% (Figure 3*H*). Based on these data, inhibition of CDK9 activity leads to a rapid decrease in transcription, which decreases mRNAs that have short half-lives and are associated with fast proliferation of cancer cells. In a longer time-frame, CDK9 inhibition leads to a decrease in the metabolic activity of cells, manifested by decreased OCR and ATP generation (Figure 1*D*). These data indicate that the highly specific CDK9 inhibitor NVP2 causes similar effects as the pan-CDK inhibitor AT7519, confirming CDK9 as a major target for AT7519 in prostate cancer cells.

Next, we assessed if inhibition of CDK9 is sufficient to induce synthetic lethality in combination with Perhexiline. Perhexiline additively enhanced the effect of NVP2 on LNCaP cell viability (Supplementary Figure 4*A*) and combination of 5 nM NVP2 with Perhexiline led to a complete growth arrest (Figure 3*I*). A low dose of NVP2 did not induce cell death on its own, but potentiated the effect of Perhexiline by over 60-fold, as measured using caspase-activation, which indicates that certain anti-proliferative effects of CDK9 inhibition are greatly enhanced by Perhexiline (Figure 3*J*). CDK9 inhibition has been reported to sensitize cancer cells to apoptosis through decreased expression of MCL1 and MYC [33,35,36]. Combining NVP2 with Perhexiline led to over 50% decrease in MYC levels but MCL1 was only modestly affected (Supplementary Figure 4*B*). In addition, and similar to the Perhexiline+AT7519 combination, we observed that Perhexiline enhances NVP2-induced DNA damage (Figure 3*B* and Supplementary Figure 4*B*). These data imply that the combination of CDK9 and FAO inhibitors does not induce apoptosis through down-regulation of anti-apoptotic proteins but rather through induction of excessive DNA damage; however, to fully define the signaling pathways involved will require a comprehensive future study.

Next, we moved on to evaluate the effect of combining CDK9 and FAO inhibitors in PC3 cells. The combination of NVP2 with Perhexiline decreased cell viability, induced cell death and caused growth arrest also in PC3 cells (Supplementary Figure 5). We wanted to further assess the ability of Perhexiline to sensitize prostate cancer cells to a clinically relevant CDK9 inhibitor. For these experiments, we selected TG02/SB1317, a compound that is currently in clinical trials [34,37]. First, we identified a dose for TG02 that had only a modest effect on cell viability as a single agent (Supplementary Figure 6*A*). Combining this low dose of TG02 with Perhexiline led to a complete loss of proliferation of both LNCaP and PC3 cells (Supplementary Figure 6*B*). To conclude, Perhexiline can enhance the effects of CDK9 inhibition on prostate cancer cell proliferation. These data confirm the model that CDK9 inhibition causes

metabolic stress to prostate cancer cells, rendering them dependent on CPT activity, which can be targeted to achieve synthetic lethality.

Discussion

CDKs are the key regulators of cell cycle and RNA-Pol II activity, and in this study we discovered that inhibition of CDK9 induces acute metabolic stress in prostate cancer cells. This is, to our knowledge, the first study to report that RNA-Pol II CTD kinase inhibition affects metabolism. Our work highlights the complex interplay between metabolism, transcription and the proteome, and shows the value of multiplatform profiling of cancer cell response to cytostatic compounds. Overall, we found that CDK9 inhibition triggers a

metabolic switch in prostate cancer cells so they rely more on CPT enzymes for growth.

Development of normal prostate tissue requires significant remodeling of mitochondrial metabolism. As a result, cells of the prostate gland do not complete the TCA cycle and secrete high levels of citrate [5,6]. This prostate-specific metabolic feature is important to promote sperm survival. However, the lack of selection pressure to maintain functionally proficient mitochondria may lead to accumulation of mitochondrial mutations and defective mitochondria. Indeed, mitochondrial genomes of normal prostate cells contain numerous mutations that are not found in other tissues of the same person [38]. Certain cancer-associated mitochondrial mutations are
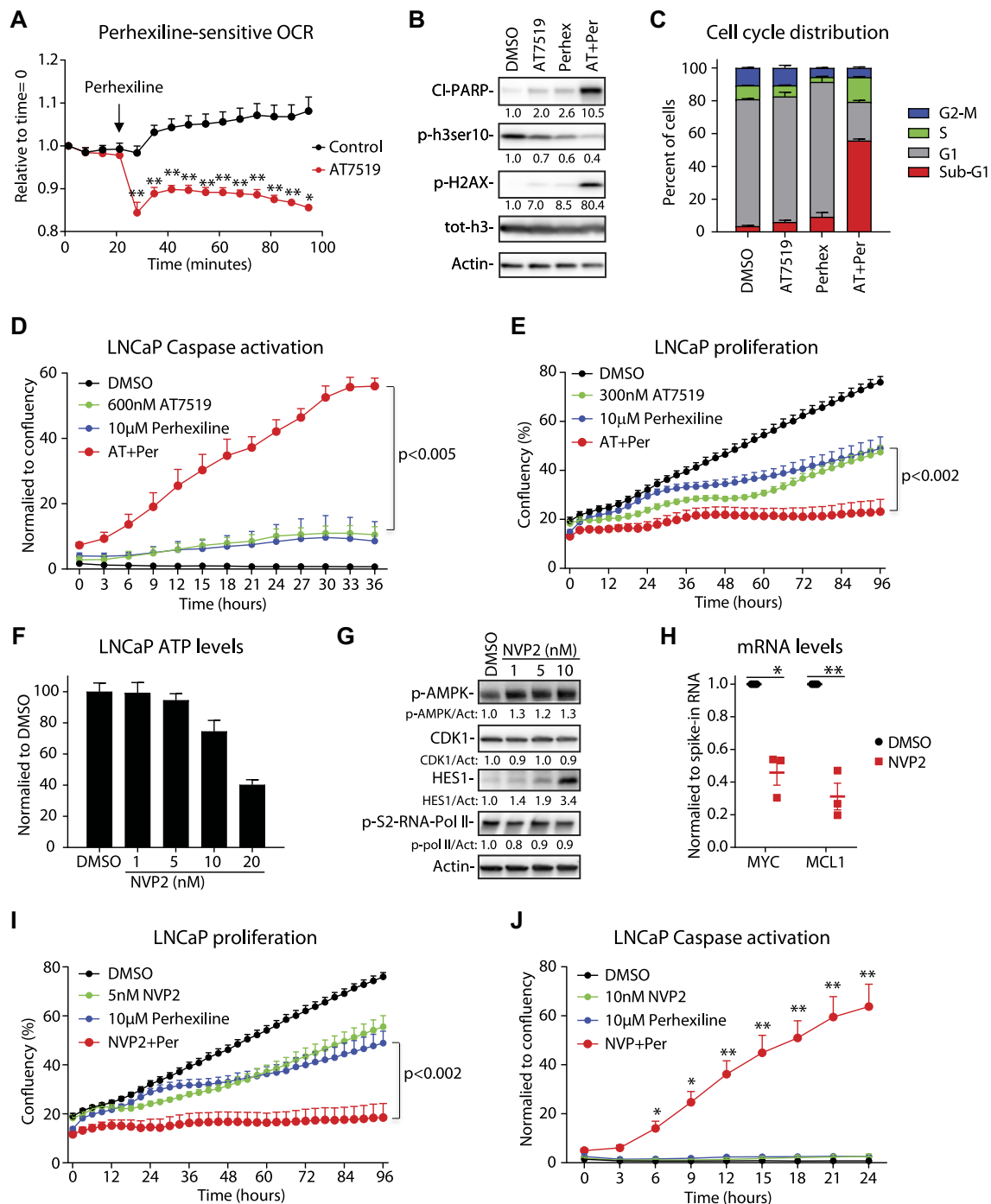
associated with aggressive disease [39], and specific mitochondrial mutations have also been reported to confer a growth advantage to otherwise isogenic prostate cancer cells [40]. Some mitochondrial mutations found in prostate cancer may also render cells more sensitive to inhibitors that affect mitochondrial function.

In this study we unexpectedly found that CDK9 activity plays a crucial role in mitochondrial function in prostate cancer cells. One report has previously linked CDK9 activity to mitochondrial dysfunction. In that case, chronic activation of CDK9 due to over-expression of the cyclin-T1 partner was shown to result in mitochondrial dysfunction in cardiac tissue [41]. Here we have found that inhibiting CDK9 activity decreased oxidative phosphorylation, rendering cells more dependent on lipids for ATP production (Figs. 1D and 3A). Therefore, inhibiting CPT activity in combination with CDK9 inhibition results in lethality in cell culture (Figure 3, D and J). Notably, the observed increase in acyl-carnitines in response to AT7519 may reflect an increased dependence on FAO or decreased ability to deacylate (Figure 2B). The latter seems more likely as we also observed a concomitant decrease in OCR (Figure 1D). Nevertheless, it may be possible to combine CDK9 and CPT inhibitors for therapeutic purposes but testing this will require challenging animal studies.

The basal transcription machinery is operational in every cell, however, inhibition of the kinases that phosphorylate RNA Pol II carboxy-terminal domain (CTD) is more toxic to cancer cells than normal cells and compounds targeting the CTD kinases are in clinical trials [34,36,42,43]. The activity of RNA Pol II is regulated at multiple levels by CDK7, CDK9 and CDK12, and transcription of different genes appears to be more reliant in the activity of only some of these kinases [13]. For example, inhibition of CDK7 and CDK9 down-regulates the expression of mRNAs with short half-life, such as the anti-apoptotic mitochondrial gene MCL1 and the oncogenic transcription factor MYC [35], as observed also in our current study (Supplementary Figure 4B). On the other hand, CDK12 appears to be particularly important for the expression of long genes, including many genes involved in the DNA damage response [44]. We observed here that the pan-CDK inhibitor AT7519 causes suppression in mitochondrial OCR and sensitizes cells to inhibition of FAO

(Figs. 1D; 3, D and E). A more thorough characterization of cancer cells' response to inhibition of specific CDKs is likely to reveal additional synthetic lethal interactions.

In conclusion, here we show that inhibition of CDK9 activity leads to suppression of mitochondrial activity and ATP production in prostate cancer cells. In the future, it will be important to identify the key mediators of this response. In more general terms, CDK9 inhibitors could be combined with other inhibitors of the key energy-sensor pathways to induce apoptosis in prostate cancer cells.

Supplementary data to this article can be found online at https://doi.org/10.1016/j.neo.2019.05.001.

Declarations of Interest

None.

References

[1] Phan LM, Yeung SC, and Lee MH (2014). Cancer metabolic reprogramming: importance, main features, and potentials for precise targeted anti-cancer therapies. *Cancer biology & medicine* **11**, 1–19.

[2] Siegel RL and Miller KD (2018). Jemal A (2018). Cancer statistics. *CA Cancer J Clin* **68**, 7–30.

[3] Oyama N, Akino H, Kanamaru H, Suzuki Y, Muramoto S, Yonekura Y, Sadato N, Yamamoto K, and Okada K (2002). 11C-acetate PET imaging of prostate cancer *Journal of nuclear medicine : official publication. Society of Nuclear Medicine* **43**, 181–186.

[4] Itkonen HM, Brown M, Urbanucci A, Tredwell G, Ho Lau C, Barfeld S, Hart C, Guldvik IJ, Takhar M, and Heemers HV, et al (2017). Lipid degradation promotes prostate cancer cell survival. *Oncotarget* **8**, 38264–38275.

[5] Barfeld SJ, Itkonen HM, Urbanucci A, and Mills IG (2014). Androgen-regulated metabolism and biosynthesis in prostate cancer. *Endocr Relat Cancer* **21**, T57–T66.

[6] Costello LC and Franklin RB (2006). The clinical relevance of the metabolism of prostate cancer; zinc and tumor suppression: connecting the dots *Molecular cancer* **5**; 2006 17.

Figure 3. CDK9 inhibitors are synthetically lethal with inhibitors of fatty acid oxidation. **A)** AT7519 renders prostate cancer cells sensitive to Perhexiline as measured using oxygen-consumption rate (OCR). A Seahorse XFe 96 analyzer was used to measure OCR of cells upon acute injection of perhexiline (indicated with an arrow). LNCaP cells were pre-treated with AT7519 for 24 hours as indicated. Data shown is an average of 3 biological replicates with SEM; *t*-test was used to evaluate statistical significance (*<.05, **<.01). **B)** Combination of 0.5 µM AT7519 with 10 µM Perhexiline induces DNA damage and cell death in LNCaP cells. Cells were treated as indicated for 24 hours and western blotting was used to detect the proteins of interest. Densitometry was used to evaluate the abundance of each protein. **C)** Combination of AT7519 with Perhexiline increases the sub-G1 population of cells. Cell cycle distribution was assessed using propidium iodide staining and flow cytometry. Data shown is an average of two biological replicates with SEM. **D)** Activation of cell death in response to AT7519 and Perhexiline treatments. The cumulative activation of Caspases 3 and 7 was recorded using live-cell imaging until 36 hours and normalized to cell confluency. Data shown is an average four biological replicate experiments with SEM; a *t*-test was used to evaluate the statistical significance. **E)** Growth rate of cells was recorded using live-cell imaging. Data shown is an average of four biological replicates with SEM and *t*-test was used to assess the statistical significance between combination treatments against any single treatment. **F)** LNCaP cells were treated with NVP2 for 24 hours and the abundance of ATP was determined using the CellTiter-Glo-assay. Data shown is an average of three technical replicates with STDEV. **G)** LNCaP cells were treated with DMSO or increasing dose of NVP2 for 24 hours and samples were analyzed using western blotting. Densitometry was used to evaluate the abundance of each protein. **H)** LNCaP cells were treated with 20 nM NVP2 for 4 hours, mRNA isolated and used for RT-qPCR. Transcript abundance was normalized to luciferase RNA that was added to each sample in the cell lysis buffer. Data shown is an average of three biological replicates with SEM and *t*-test was used to assess the statistical significance. **I)** Growth rate of cells was recorded using live-cell imaging. Data shown is an average of four biological replicates with SEM and *t*-test was used to assess the statistical significance between combination treatments against any single treatment. **J)** Activation of cell death in response to AT7519 and Perhexiline treatments. The cumulative activation of Caspases 3 and 7 was recorded using live-cell imaging until 36 hours and normalized to cell confluency. Data shown is an average of four biological replicate experiments with SEM and *t*-test was used to evaluate the statistical significance (*<.05, **<.01).

[7] Costello LC and Franklin RB (1981). Aconitase activity, citrate oxidation, and zinc inhibition in rat ventral prostate. *Enzyme* **26**, 281–287.

[8] Onodera Y, Nam JM, and Bissell MJ (2014). Increased sugar uptake promotes oncogenesis via EPAC/RAP1 and O-GlcNAc pathways. *J Clin Invest* **124**, 367–384.

[9] Wang Z, Fan M, Candas D, Zhang TQ, Qin L, Eldridge A, Wachsmann-Hogiu S, Ahmed KM, Chromy BA, and Nantajit D, et al (2014). Cyclin B1/Cdk1 coordinates mitochondrial respiration for cell-cycle G2/M progression. *Dev Cell* **29**, 217–232.

[10] Lee Y, Dominy JE, Choi YJ, Jurczak M, Tolliday N, Camporez JP, Chim H, Lim JH, Ruan HB, and Yang X, et al (2014). Cyclin D1-Cdk4 controls glucose metabolism independently of cell cycle progression. *Nature* **510**, 547–551.

[11] Wang H, Nicolay BN, Chick JM, Gao X, Geng Y, Ren H, Gao H, Yang G, Williams JA, and Suski JM, et al (2017). The metabolic function of cyclin D3-CDK6 kinase in cancer cell survival. *Nature* **546**, 426–430.

[12] Hsin JP and Manley JL (2012). The RNA polymerase II CTD coordinates transcription and RNA processing. *Genes Dev* **26**, 2119–2137.

[13] Harlen KM and Churchman LS (2017). The code and beyond: transcription regulation by the RNA polymerase II carboxy-terminal domain. *Nat Rev Mol Cell Biol* **18**, 263–273.

[14] Malumbres M and Barbacid M (2009). Cell cycle, CDKs and cancer: a changing paradigm. *Nat Rev Cancer* **9**, 153–166.

[15] Gordon V, Bhadel S, Wunderlich W, Zhang J, Ficarro SB, Mollah SA, Shabanowitz J, Hunt DF, Xenarios I, and Hahn WC, et al (2010). CDK9 regulates AR promoter selectivity and cell growth through serine 81 phosphorylation. *Mol Endocrinol* **24**, 2267–2280.

[16] Rahl PB, Lin CY, Seila AC, Flynn RA, McCuine S, Burge CB, Sharp PA, and Young RA (2010). c-Myc regulates transcriptional pause release. *Cell* **141**, 432–445.

[17] Huang CH, Lujambio A, Zuber J, Tschaharganeh DF, Doran MG, Evans MJ, Kitzing T, Zhu N, de Stanchina E, and Sawyers CL, et al (2014). CDK9-mediated transcription elongation is required for MYC addiction in hepatocellular carcinoma. *Genes Dev* **28**, 1800–1814.

[18] Konig A, Schwartz GK, Mohammad RM, Al-Katib A, and Gabrilove JL (1997). The novel cyclin-dependent kinase inhibitor flavopiridol downregulates Bcl-2 and induces growth arrest and apoptosis in chronic B-cell leukemia lines. *Blood* **90**, 4307–4312.

[19] Itkonen HM, Minner S, Guldvik IJ, Sandmann MJ, Tsourlakis MC, Berge V, Svindland A, Schlomm T, and Mills IG (2013). O-GlcNAc transferase integrates metabolic pathways to regulate the stability of c-MYC in human prostate cancer cells. *Cancer Res* **73**, 5277–5287.

[20] Squires MS, Feltell RE, Wallis NG, Lewis EJ, Smith DM, Cross DM, Lyons JF, and Thompson NT (2009). Biological characterization of AT7519, a small-molecule inhibitor of cyclin-dependent kinases, in human tumor cell lines. *Mol Cancer Ther* **8**, 324–332.

[21] Lopez-Mejia IC, Lagarrigue S, Giralt A, Martinez-Carreres L, Zanou N, Denechaud PD, Castillo-Armengol J, Chavey C, Orpinell M, and Delacuisine B, et al (2017). CDK4 Phosphorylates AMPKalpha2 to Inhibit Its Activity and Repress Fatty Acid Oxidation *Molecular cell*, 68; 2017 336–349 e336.

[22] Lin SC and Hardie DG (2018). AMPK: Sensing Glucose as well as Cellular Energy Status. *Cell Metab* **27**, 299–313.

[23] Houten SM and Wanders RJ (2010). A general introduction to the biochemistry of mitochondrial fatty acid beta-oxidation. *J Inherit Metab Dis* **33**, 469–477.

[24] Lionetti V, Stanley WC, and Recchia FA (2011). Modulating fatty acid oxidation in heart failure. *Cardiovasc Res* **90**, 202–209.

[25] Rupp H, Zarain-Herzberg A, and Maisch B (2002). The use of partial fatty acid oxidation inhibitors for metabolic therapy of angina pectoris and heart failure. *Herz* **27**, 621–636.

[26] Lilly K, Chung C, Kerner J, VanRenterghem R, and Bieber LL (1992). Effect of etomoxiryl-CoA on different carnitine acyltransferases. *Biochem Pharmacol* **43**, 353–361.

[27] Schlaepfer IR, Glode LM, Hitz CA, Pac CT, Boyle KE, Maroni P, Deep G, Agarwal R, Lucia SM, and Cramer SD, et al (2015). Inhibition of Lipid Oxidation Increases Glucose Metabolism and Enhances 2-Deoxy-2-[(18)F]Fluoro-D-Glucose Uptake

[28] in Prostate Cancer Mouse Xenografts *Molecular imaging and biology : MIB : the official publication of the Academy of. Mol Imaging* **17**, 529–538.

[28] Agius L, Meredith EJ, and Sherratt HS (1991). Stereospecificity of the inhibition by etomoxir of fatty acid and cholesterol synthesis in isolated rat hepatocytes. *Biochem Pharmacol* **42**, 1717–1720.

[29] Zarain-Herzberg A, Rupp H, Elimban V, and Dhalla NS (1996). Modification of sarcoplasmic reticulum gene expression in pressure overload cardiac hypertrophy by etomoxir. *FASEB J* **10**, 1303–1309.

[30] Yao CH, Liu GY, Wang R, Moon SH, Gross RW, and Patti GJ (2018). Identifying off-target effects of etomoxir reveals that carnitine palmitoyltransferase I is essential for cancer cell proliferation independent of beta-oxidation. *PLoS Biol* **16**e2003782.

[31] Pike LS, Smift AL, Croteau NJ, Ferrick DA, and Wu M (2011). Inhibition of fatty acid oxidation by etomoxir impairs NADPH production and increases reactive oxygen species resulting in ATP depletion and cell death in human glioblastoma cells. *Biochim Biophys Acta* **1807**, 726–734.

[32] Bester AC, Roniger M, Oren YS, Im MM, Sarni D, Chaoat M, Bensimon A, Zamir G, Shewach DS, and Kerem B (2011). Nucleotide deficiency promotes genomic instability in early stages of cancer development. *Cell* **145**, 435–446.

[33] Olson CM, Jiang B, Erb MA, Liang Y, Doctor ZM, Zhang Z, Zhang T, Kwiatkowski N, Boukhali M, and Green JL, et al (2018). Pharmacological perturbation of CDK9 using selective CDK9 inhibition or degradation. *Nat Chem Biol* **14**, 163–170.

[34] Sonawane YA, Taylor MA, Napoleon JV, Rana S, Contreras JI, and Natarajan A (2016). Cyclin Dependent Kinase 9 Inhibitors for Cancer Therapy. *J Med Chem* **59**, 8667–8684.

[35] Gregory GP, Hogg SJ, Kats LM, Vidacs E, Baker AJ, Gilan O, Lefebure M, Martin BP, Dawson MA, and Johnstone RW, et al (2015). CDK9 inhibition by dinaciclib potently suppresses Mcl-1 to induce durable apoptotic responses in aggressive MYC-driven B-cell lymphoma in vivo. *Leukemia* **29**, 1437–1441.

[36] Boffo S, Damato A, Alfano L, and Giordano A (2018). CDK9 inhibitors in acute myeloid leukemia. *Journal of experimental & clinical cancer research : CR* **37**, 36.

[37] Goh KC, Novotny-Diermayr V, Hart S, Ong LC, Loh YK, Cheong A, Tan YC, Hu C, Jayaraman R, and William AD, et al (2012). TG02, a novel oral multi-kinase inhibitor of CDKs, JAK2 and FLT3 with potent anti-leukemic properties. *Leukemia* **26**, 236–243.

[38] Parr RL, Dakubo GD, Crandall KA, Maki J, Reguly B, Aguirre A, Wittock R, Robinson K, Alexander JS, and Birch-Machin MA, et al (2006). Somatic mitochondrial DNA mutations in prostate cancer and normal appearing adjacent glands in comparison to age-matched prostate samples without malignant histology. *The Journal of molecular diagnostics : JMD* **8**, 312–319.

[39] Hopkins JF, Sabelnykova VY, Weischenfeldt J, Simon R, Aguiar JA, Alkallas R, Heisler LE, Zhang J, Watson JD, and Chua MLK, et al (2017). Mitochondrial mutations drive prostate cancer aggression. *Nat Commun* **8**, 656.

[40] Arnold RS, Sun CQ, Richards JC, Grigoriev G, Coleman IM, Nelson PS, Hsieh CL, Lee JK, Xu Z, and Rogatko A, et al (2009). Mitochondrial DNA mutation stimulates prostate cancer growth in bone stromal environment. *Prostate* **69**, 1–11.

[41] Sano M, Wang SC, Shirai M, Scaglia F, Xie M, Sakai S, Tanaka T, Kulkarni PA, Barger PM, and Youker KA, et al (2004). Activation of cardiac Cdk9 represses PGC-1 and confers a predisposition to heart failure. *EMBO J* **23**, 3559–3569.

[42] Kumar SK, LaPlant B, Chng WJ, Zonder J, Callander N, Fonseca R, Fruth B, Roy V, Erlichman C, and Stewart AK, et al (2015). Dinaciclib, a novel CDK inhibitor, demonstrates encouraging single-agent activity in patients with relapsed multiple myeloma. *Blood* **125**, 443–448.

[43] Tong WG, Chen R, Plunkett W, Siegel D, Sinha R, Harvey RD, Badros AZ, Popplewell L, Coutre S, and Fox JA, et al (2010). Phase I and pharmacologic study of SNS-032, a potent and selective Cdk2, 7, and 9 inhibitor, in patients with advanced chronic lymphocytic leukemia and multiple myeloma. *J Clin Oncol* **28**, 3015–3022.

[44] Krajewska M, Dries R, Grassetti AV, Dust S, Gao Y, Huang H, Sharma B, Day DS, Kwiatkowski N, and Pomaville M, et al (2019). CDK12 loss in cancer cells affects DNA damage response genes through premature cleavage and polyadenylation. *Nat Commun* **10**, 1757.